Synsint Research Group

Available online at www.synsint.com

Synthesis and Sintering

ISSN 2564-0186 (Print), **ISSN** 2564-0194 (Online)

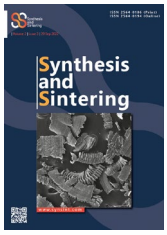

Research article

Role of SPS temperature and holding time on the properties of Ti_3AlC_2-doped TiAl composites

Maryam Akhlaghi [a], **Esmaeil Salahi** [b,*], **Seyed Ali Tayebifard** [b], **Gert Schmidt** [c]

[a] *Semiconductors Department, Materials and Energy Research Center (MERC), Karaj, Iran*
[b] *Ceramics Department, Materials and Energy Research Center (MERC), Karaj, Iran*
[c] *Faculty of Mechanical, Process and Energy Engineering, TU Bergakademie, Freiberg, Germany*

A B S T R A C T

In order to study the effects of sintering conditions on the properties of TiAl-based materials, two different compositions (TiAl-15 wt% Ti_3AlC_2 and TiAl-25 wt% Ti_3AlC_2) were chosen and manufactured by spark plasma sintering at 900 °C/7 min and 1000 °C/15 min. The results showed that increasing the MAX phase content had a positive effect on the relative density and mechanical properties, but simultaneous increasing the temperature and holding time is more effective in the improvement of properties. For TiAl-15 wt% Ti_3AlC_2 sample, the relative density, Vickers hardness, fracture toughness, and bending strength increased from 92.3%, 3.6 GPa, 10.9 MPa.m$^{1/2}$, and 206 MPa to 95.2%, 4.5 GPa, 12.0 MPa.m$^{1/2}$, and 336 MPa, respectively, as the sintering temperature and holding time increased from 900 °C/7 min to 1000 °C/15 min. In the case of the TiAl-25 wt% Ti_3AlC_2 sample, increasing the sintering temperature and holding time from 900 °C/7 min to 1000 °C/15 min led to the improvement of relative density, Vickers hardness, fracture toughness, and bending strength from 92.8%, 4.1 GPa, 11.2 MPa.m$^{1/2}$, and 270 MPa to 97.5%, 4.6 GPa, 11.8 MPa.m$^{1/2}$, and 340 MPa, respectively.

KEYWORDS

$TiAl-Ti_3AlC_2$ composites
Relative density
Flexural strength
Hardness
Fracture toughness

OPEN ACCESS

1. Introduction

TiAl-based materials are drawn the wide attention of researchers due to their privileged features such as low density, high melting temperature, good creep and oxidation resistance, and good corrosion properties. These unique properties have made them suitable choices to utilize in various high-temperature structural usages and automobiles [1–4]. However, the development and application of such materials have been restricted by their shortcomings like weak formability and low-temperature ductility [5–7]. Therefore, utilizing a suitable consolidation technique and reinforcement introduction or changing the composition is an appropriate approach to overcome such weaknesses [8–11]. Spark plasma sintering (SPS) as a newly developed route that uses a direct or pulsed current and external load, simultaneously, can be employed to manufacture TiAl-based composites with developed microstructure [12–15]. The microstructure and mechanical properties of titanium aluminides can be controlled by the SPS temperature. The changes are observed in the microstructure of TiAl as the temperature increases [16–19]. Spark plasma sintering of pre-alloyed Ti-47Al-2Cr-2Nb [5], Ti-46Al-9Nb [20], Ti-44Al-2Cr-2Nb-1B [5], and Ti-48Al-2Cr-2Nb [21] has led to the achievement of different lamellar, two-phased (γ+α2), and duplex microstructures depending on initial powder composition and the processing temperature. Similar microstructural concurrence has been reported for pre-alloyed powders of Ti–43.9Al–4Nb–0.95Mo–0.1B as the function of sintering temperature. Manufacturing of pre-alloyed Ti-43Al-5Nb-2V-1Y powders by the SPS

* Corresponding author. *E-mail address:* e-salahi@merc.ac.ir (E. Salahi)
Received 26 December 2021; Received in revised form 30 September 2022; Accepted 30 September 2022.

https://doi.org/10.53063/synsint.2022.2383

process results in nearly lamellar, fully lamellar, and duplex microstructures with temperature change [22]. It should be mentioned that the extreme growth of TiAl grains as a result of increasing the processing temperature was observed in the microstructure of SPSed Ti-47Al powders, which led to a decrease in yield strength and hardness, but an eligible improvement of ductility [23]. Moderate ductility and excellent creep resistance were achieved as a result of the formation of a nearly lamellar microstructure [24].

In recent decades, composites making has been recognized as a suitable approach for improving the mechanical and physical properties of materials. Therefore, the combination of MAX phases and intermetallic components has been studied to make composites [25]. It is worth noting that MAX phases are a newly developed group of materials with a hexagonal layered structure having both metallic and ceramic features at the same time. Because of their unique properties such as a high melting point, superior strength, good electrical and thermal conductivity, and thermal stability, these materials have received the growing attention of researchers to use in structural applications [26–28]. TiAl-Ti_2AlC composites have been manufactured by spark plasma sintering of TiC, Al, and Ti powders. It is known that the TiC content in the powder mixture dramatically affects the phase evolution and microstructure development of the SPSed samples [29]. Mechanical alloying and spark plasma sintering has been employed to synthesize TiAl-Ti_2AlC composites utilizing Al, Ti, and CNTs to obtain a composite with a microstructure consisting of interpenetrating networks of Ti_2AlC and equiaxed TiAl grains. Coarsening of TiAl grains is observed when the SPS temperature increases from 950 to 1150 °C, resulting in the degradation of mechanical properties [30]. Ball-milling and spark plasma sintering of graphene and pre-alloyed Ti-48Al-2Nb-2Cr powder were utilized to manufacture TiAl-Ti_2AlC nanocomposites, where the Ti_2AlC precipitates were uniformly dispersed in the fully lamellar microstructure. In mentioned research, the effect of microstructure evolution on oxidation resistance is discussed [31].

In the present work, in order to assess the effects of temperature and soaking time, TiAl-based composites reinforced with 15 and 25 wt% Ti_3AlC_2 were spark plasma sintered under an external pressure of 40 MPa at different temperatures of 900 and 1000 °C with different holding time of 7 and 15 min.

2. Experimental

Commercial elemental powders of aluminum and titanium as well as the synthesized MAX phase of Ti_3AlC_2 were chosen as the initial materials for the preparation of TiAl-Ti_3AlC_2 composite samples. Metallic Ti and Al powders in equal molar ratios were utilized as raw precursors for the in-situ synthesis of intermetallic TiAl by SPS procedure. To prepare the MAX phase of Ti_3AlC_2, a powder mixture of graphite, Al, and Ti was mechanically-activated and then processed by the self-propagating high-temperature synthesis (SHS) (details in Ref. [32]). It should be stated that the purity of the obtained Ti_3AlC_2 MAX phase is 85 wt%, in other words, the final powder contains 15 wt% TiC, which is obtained as an impurity during the synthesis of Ti_3AlC_2. Ti_3AlC_2 powder was added in different contents of 15 and 25 wt% as the reinforcement in the TiAl matrix. The weighted powder mixtures of Ti_3AlC_2, Al, and Ti were ball-milled at 300 rpm for 60 min. After that, each powder mixture was divided into two parts to consolidate under different sintering conditions (soaking time of 7 and 15 min, SPS temperature of 900 and 1000 °C). Prepared powder mixtures are poured into an appropriate graphite mold covered with a flexible graphite sheet to minimize sticking the powder composites to the die.

After inserting the die in the spark plasma sintering furnace (model: 20T-10), an initial minimum pressure (~8 MPa) was applied (details in Ref. [33]). A set of TiAl-15 wt% Ti_3AlC_2 (sample 1) and TiAl-25 wt% Ti_3AlC_2 (sample 2) was spark plasma sintered at 900 °C for 7 min under an external pressure of 40 MPa, and another set of TiAl-15 wt% Ti_3AlC_2 (sample 3) and TiAl-25 wt% Ti_3AlC_2 (sample 4) was spark plasma sintered at different conditions (temperature of 1000 °C for 15 min under the same pressure). Grinding surfaces of as-SPSed samples was performed by a diamond grinding disk to eliminate the graphite foil. Measurement of bulk density was performed employing Archimedes method. Theoretical densities of as-SPSed samples were calculated by the rule of mixture. The ratio of bulk density to the theoretical density of as-SPSed samples reported the relative densities of as-SPSed samples. For measurement of bending strength, the rod-shaped samples were cut in dimensions of $3 \times 4 \times 25$ mm^3 with a wire cut tool (Charmilles Robofill 310 wire EDM) equipped a wire, which had 0.25 mm thickness. The surfaces of the samples and the cut parts of rod-shaped samples were polished for Vickers hardness and the bending strength tests, respectively. The three-point method was employed to determine the bending strength of as-SPSed specimens at room temperature utilizing a crosshead loading rate of 0.5 mm/min (ASTM C-1161- 02C). To measure the fracture toughness of as-SPSed samples, the rods (with dimensions of $3 \times 4 \times 25$ mm^3) were sharply notched with a depth of 0.4 of the specimen width and tested by single edge notched beam (SENB) method. A three-point bending test device with a constant crosshead speed of 0.5 mm/min and a fixed length of the gauge (20 mm) was used to test the notched rods. Finally, the assessment of fracture toughness values was performed with the following formula:

$$K_{IC} = \frac{3PLa^{\frac{1}{2}}}{2BW^2} \times Y \quad (1)$$

where L is gauge length, P is the maximum applied load, W is the width of the sample, a is the depth of the notch, B is rod thickness, and Y is geometric constants.

The Vickers hardness of as-SPSed specimens was evaluated by indentation method through exerting a 2 kg of load (19.6 N) utilizing the Vickers diamond pyramid. The crack propagation paths created during the SENB test were investigated through field emission scanning electron microscopy (Mira3, Tescan).

3. Results and discussion

Table 1 shows the composition, sintering conditions, relative density, and mechanical properties (bending strength, Vickers hardness, and fracture toughness) of as-SPSed composite samples. Fig. 1 shows the measured relative density values of as-SPS samples. As it is clear from Fig. 1, increasing the content of Ti_3AlC_2 from 15 wt% to 25 wt% has a positive influence on the densification, so that the relative density for the composites sintered at 900 °C for 7 min and for composites sintered at 1000 °C for 15 min improved by about 0.5% and about 2.5%, respectively. As can be seen, changing the SPS conditions has led to changing the relative density value. The maximum value of relative density (97.52%) belongs to sample 4 including 25 wt% Ti_3AlC_2, which was sintered at a higher temperature and time. An increase in

Table 1. Composition and properties of the spark plasma sintered TiAl-based composites.

Sample no.	Composition	Sintering conditions		Relative density (%)	Bending strength (MPa)	Vickers hardness (GPa)	Fracture toughness (MPa.m$^{1/2}$)
		Temperature (°C)	Time (min)				
1	(TiAl-15 wt% Ti_3AlC_2)	900	7	92.34 ± 0.23	250 ± 21	3.7 ± 0.7	11.75 ± 0.52
2	(TiAl-25 wt% Ti_3AlC_2)	900	7	92.78 ± 0.32	270 ± 42	4.1 ± 0.5	11.21 ± 0.33
3	(TiAl-15 wt% Ti_3AlC_2)	1000	15	95.21 ± 0.37	336 ± 21	4.5 ± 0.2	11.98 ± 0.10
4	(TiAl-25 wt% Ti_3AlC_2)	1000	15	97.52 ± 0.28	340 ± 19	4.6 ± 0.40	11.81 ± 0.2

temperature has a direct effect on the processing kinetics and leads to an increase in the diffusion rate of atoms and the formation of bonds in the structure. Also, increasing the holding time creates more opportunities for atoms to diffuse and increase the density of the samples.

To investigate the effect of temperature and the dwell time of the SPS process on the phase evolution of as-sintered samples, their XRD patterns were analyzed, which can be seen in Fig. 2. It seems that increasing the temperature and holding time of SPS has not changed the crystalline phases and new phases have not formed. TiAl as the main phase and Ti_3AlC_2 along with Ti_3Al and Ti_2AlC as the in-situ synthesized phases are identified in the microstructure of the samples spark plasma sintered at 1000 °C for 15 min under 40 MPa.

The displacement-time-temperature (DTT) diagrams of samples 3 and 4 made during the SPS process are demonstrated in Fig. 3. The DTT diagrams displaying the temperature variations as well as the shrinkage amount in the samples over time are similar to samples 1 and 2 (see Ref. [33]). Two slope changes can be seen in Figs. 3a and 3b. 17 minutes after the start of the processing when the temperature reached ~450 °C, the first change is observed, which could be related to Al melting at the beginning of heating. It is worthy to mention that aluminum melts at 660 °C, but the real temperature inside the graphite mold and between the powder particles is different from the temperature written in the diagram measured by an infrared sensor (thermocouple) located outside of the mold. The reason for this phenomenon is that the local temperature can quickly rise to a much higher than the temperature measured by the thermocouple [34], thereby, melting of Al may be possible. Above ~450 °C, the slope of the temperature diagram increases up to the maximum temperature (1000 °C). The beginning of the exothermic reaction of TiAl formation is the reason for aforesaid occurrences. Besides, the TiAl phase reacts with the TiC phase as a byproduct of the formation of Ti_3AlC_2 leading to the synthesis of the Ti_2AlC MAX phase, which is also exothermic. Such an exothermic reaction increases the slope of the diagram.

Also, as can be observed in Fig. 3, the shrinkage behavior of both samples is similar. According to the relevant diagram, first, the slope of shrinkage has a gentle increasing trend up to 15 min, and the total amount of sample shrinkage until the 15th min is 1 mm. As the aluminum starts to melt, the samples shrink by a further 3.5 mm. After that, there is no compaction in the specimens for up to 30 min. Owing to the applied final pressure and the progression of sintering; a sudden increase in the shrinkage curve from 4.5 to 5.5 mm can be seen.

Derivatives of DTT diagrams were utilized to determine the accurate time and temperature of synthesis and to understand the sintering progress more clearly. Therefore, two graphs including displacement rate versus time and displacement rate versus temperature for samples

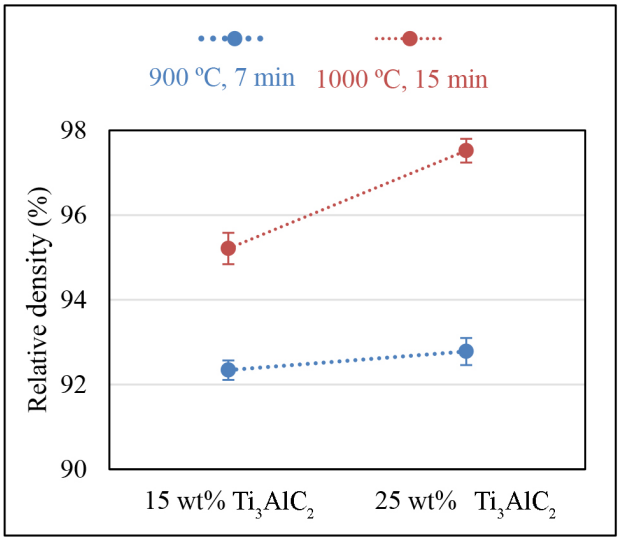

Fig. 1. Relative densities of as-SPSed composite samples.

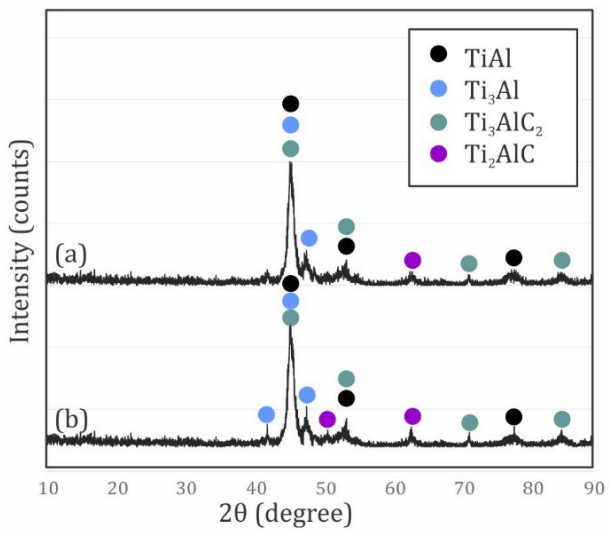

Fig. 2. XRD patterns of a) sample 3 and b) sample 4.

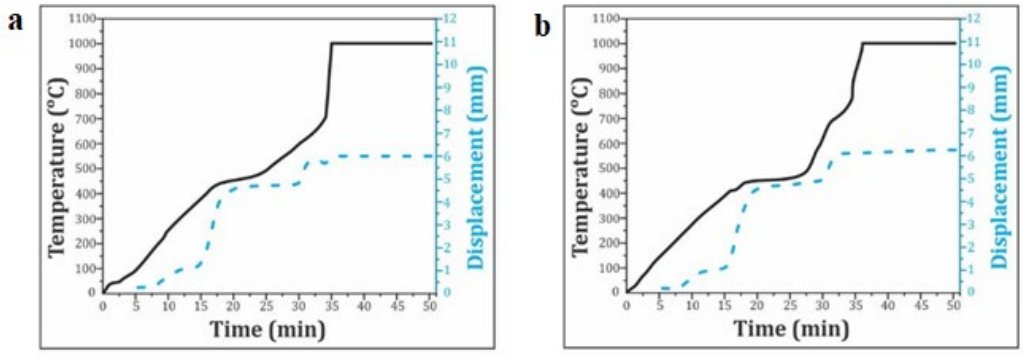

Fig. 3. DTT variations during the spark plasma sintering of a) sample 3 and b) sample 4.

3 and 4 were also plotted as shown in Figs. 4 and 5, respectively. There are a few slight peaks and 2 sharp peaks in the displacement rate diagram vs. time shown in Fig. 4. It seems that the initial applied load causes the first weak peaks to appear in times of about 6 and 11 min and the Al melting is the reason of the first sharp peak that can be observed between 16 and 23 min. The dissolution of titanium powder in molten Al and the formation of TiAl seem to be the reasons that no specific peak is observed in the time range of 25 to 32 minutes. Also, the Ti_2AlC MAX phase is synthesized by the chemical reaction between the in-situ formed TiAl matrix and titanium carbide as the byproduct of the Ti_3AlC_2 formation. Eventually, the second sharp peak observed in 32.5th min is attributed to the maximum applied load, which results in the completion of the densification and sintering process.

Fig. 5 shows a few slight peaks and two sharp peaks in the displacement rate versus temperature diagram. As can be seen in Fig. 5, the sharp peak appears at about 400 °C. This phenomenon can be related to the Al melting, which drastically affects the amount of mandrel displacement. No peak is detected at the temperature range of 460 to 600 °C that may be related to the formation of the TiAl matrix and synthesis of the Ti_2AlC MAX phase because of a chemical reaction between the TiC phase as a byproduct of Ti_3AlC_2 formation and TiAl matrix phase. The application of maximum external load at the temperature of 650 °C that results in the displacement and movement of the mandrels, more compaction of the powder mixture, and full densification, is the reason of appearing the relatively sharp peak at this temperature. It should be noted that the appearance of the first minor peaks is attributed to the applied initial load.

Fig. 6 presents the bending strength of as-sintered samples according to their sintering conditions. As can be seen in Fig. 6, on one hand, increasing the amount of Ti_3AlC_2 has a positive influence on the bending strength, on the other hand, changing SPS conditions (increasing SPS temperature and holding time) results in higher bending strength. Bending strength can be influenced by different items like grain size, microstructural defects, additive type, and relative density. Increasing the Ti_3AlC_2 content not only improves the sinterability and densification but also prevents grain growth by being located at grain boundaries and limiting their movements. It should be mentioned that Ti_2AlC, as the byproduct of Ti_3AlC_2, also has the role of inhibiting grain growth, which increases with an increase in the Ti_3AlC_2 content. Therefore, the amount of Ti_3AlC_2 has a direct influence on the bending strength of as-SPSed composite samples, so that bending strength of as-SPSed samples increases from 250 to 270 MPa as the Ti_3AlC_2 increased from 15 to 25 wt%. As can be seen in Fig. 6, the bending strength of sample 3 (TiAl-15 wt% Ti_3AlC_2) and sample 4 (TiAl-25 wt% Ti_3AlC_2), sintered at higher temperature and longer time, is more than those of samples 1 and 2. As it is discussed before, increasing the sintering temperature and holding time leads to the enhancement of relative density, which has a direct effect on the bending strength. Bending strength values were obtained as 336 and

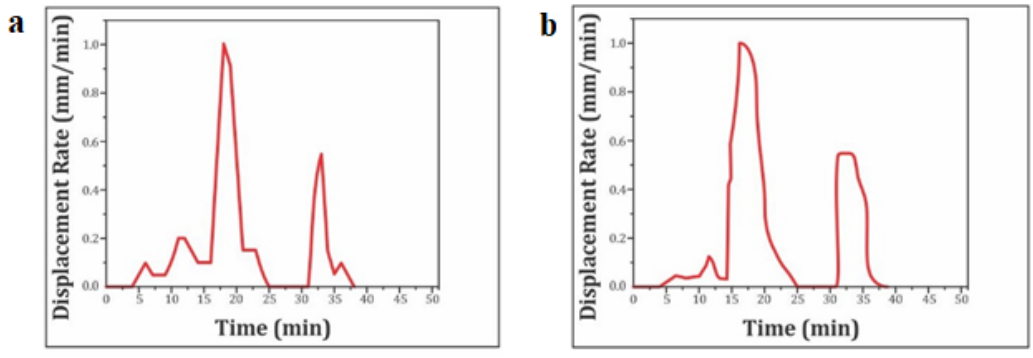

Fig. 4. Displacement rate vs. time for a) sample 3 and b) sample 4.

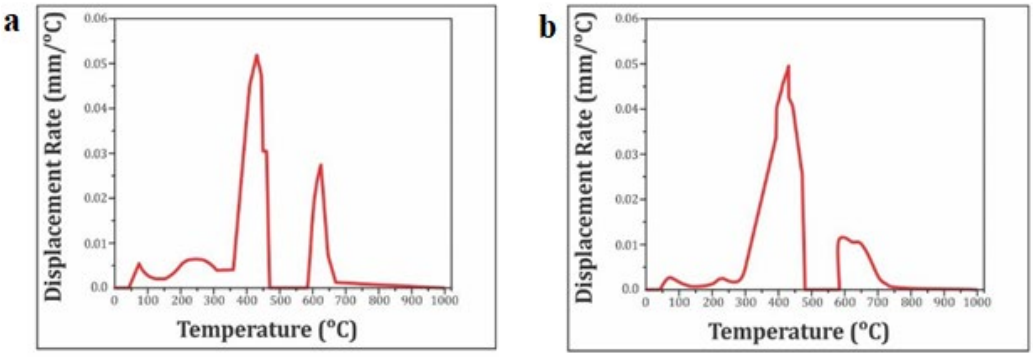

Fig. 5. Displacement rate vs. temperature for a) sample 3 and b) sample 4.

340 MPa for samples 3 and 4, respectively. Although, the measured bending strength values of as-SPSed samples are less than those reported by other researchers [35, 36]. Also, compared to the bending strength of the TiAl matrix phase (460 MPa) [37] and Ti_3AlC_2 additive [38], this property of as-SPSed samples is lower which can be related to the presence of porosities in their microstructure. In the case of sample 4, it seems that increasing the Ti_3AlC_2 content resulted in agglomerates formation of these MAX phases acting as the defects; therefore, the bending strength of this sample could not be increased more than 340 MPa. It is worthy to say that the obtained bending strength of 340 MPa for sample 4 with a relative density of 97.5 is in good agreement with that of the TiAl-based composite (360 MPa) with a relative density of 99% reported by other researchers [37].

The values of Vickers hardness of as-SPSed composite samples are shown in Fig. 7. As can be seen in Table 1 and Fig. 7, simultaneous increase of time, temperature, and content of Ti_3AlC_2 improve hardness. Increasing the Ti_3AlC_2 from 15 to 25 wt% leads to an improvement of Vickers hardness from 3.7 to 4.1 GPa. Meanwhile, increasing the holding time and processing temperature also helps the additive content to further improve this property, so that the Vickers hardness values for TiAl-15 wt% Ti_3AlC_2 and TiAl-25 wt% Ti_3AlC_2 samples, sintered at 1000 °C for 15 min, are calculated as 4.5 and 4.6 GPa, respectively. Vickers hardness is a feature of the material showing its resistance against plastic deformation when the load is applied and generally measured by indentation test. It should be mentioned that pores and porosities have less resistance against applied mechanical load; therefore, Vickers hardness of fully-dense materials is higher than that of porous materials. As previously mentioned the role of Ti_3AlC_2 in inhibiting grain growth, increasing the amount of this MAX phase leads to the modification of the microstructure and thus the improvement of Vickers hardness. Also, an increasing the Ti_3AlC_2 content leads to further Ti_2AlC formation during the SPS process. This phase can not only act as the inhibitor of the growth of matrix grains but also hardens as-SPSed samples owing to its intrinsic hardness (4.5 GPa) [39] that is higher than that of the Ti_3AlC_2 phase (2.7 GPa) [40]. According to Table 1

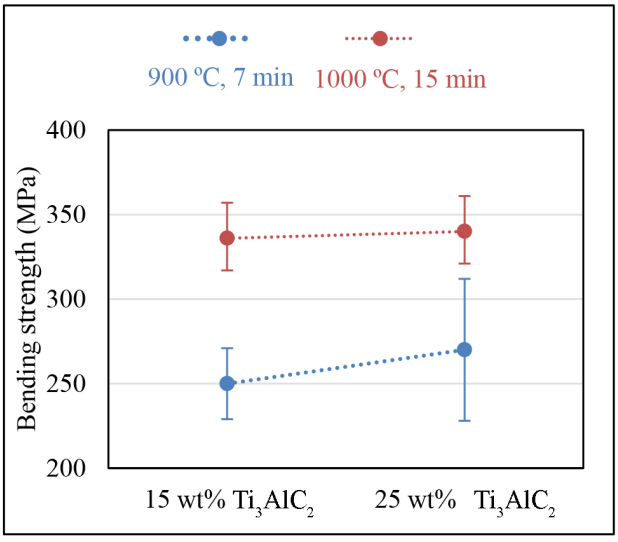

Fig. 6. Bending strength of as-SPSed composite samples.

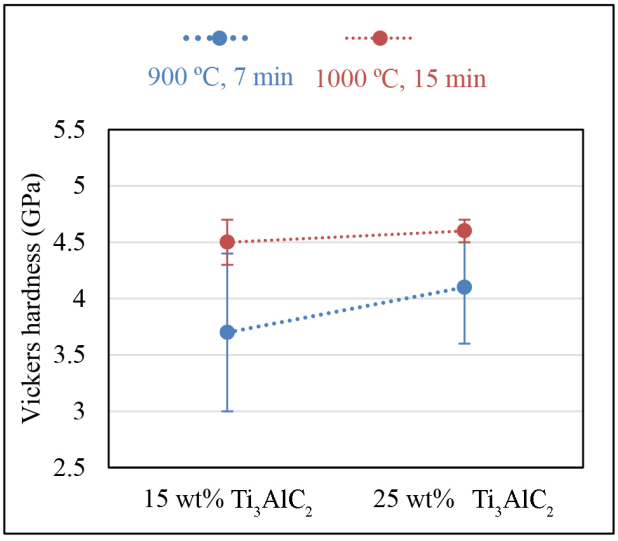

Fig. 7. Vickers hardness of as-SPSed composite samples.

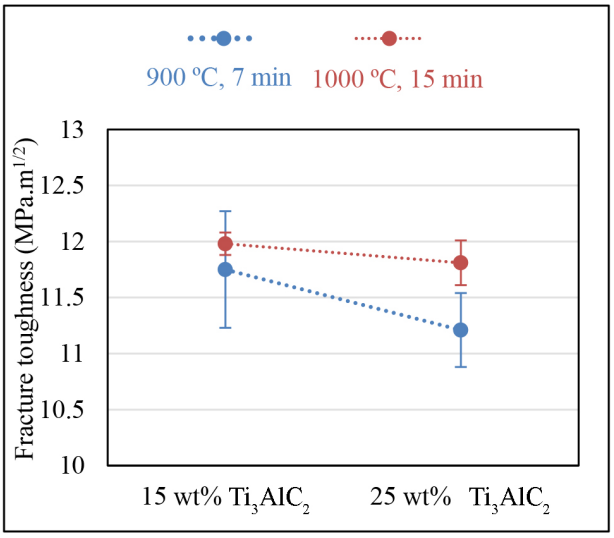

Fig. 8. Fracture toughness of as-SPSed composite samples.

and Fig. 7, changing the sintering temperature and holding time in samples 3 and 4 not only enhances the densification and bending strength but also improves the Vickers hardness. As it is mentioned before, increasing the temperature and holding time provides the chance for the penetration of atoms and the rearrangement of particles leading to improvement of sinterability and densification. Therefore, the enhancement of Vickers hardness of samples 3 and 4 can be a result of density improvement. As can be seen in Fig. 7, increasing the amount of Ti_3AlC_2 to 25 wt% in samples sintered at 1000 °C for 15 min has a slight effect on improving the hardness, so that only about 2% is able to improve the hardness. It seems that this observation is because of the formation of some agglomerates owing to the presence of more Ti_3AlC_2, higher temperature, and longer holding time.

Fig. 8 demonstrated the fracture toughness values of the as-SPSed sample. It is clear that the changing trend of the fracture toughness values of the as-SPSed samples is slightly different from the changing trend of their flexural strength and Vickers hardness values. According to Fig. 8, the value of the fracture toughness is decreased from 11.75 to 11.21 for samples sintered at 900 °C for 7 min and from 11.98 to 11.81 $MPa.m^{1/2}$ for samples sintered at 1000 °C for 15 min by increasing in the amount of Ti_3AlC_2 additive from 15 to 25 wt%, respectively. According to the standard deviation calculated for samples, it seems that the obtained fracture toughness values do not differ much. But these values of fracture toughness are remarkably higher than those reported for different ceramic matrix composites [41–44].

FESEM fractographs of samples 2 and 4 fractured in the SENB test and related cracks are presented in Fig. 9. As can be observed in Fig. 9, some toughening mechanisms such as crack deflection, crack branching, and crack bridging occur in as-SPSed samples. Considering the ability of MAX phases with a layered structure and high aspect ratio to absorb crack energy, the appropriate toughness of these samples seems reasonable.

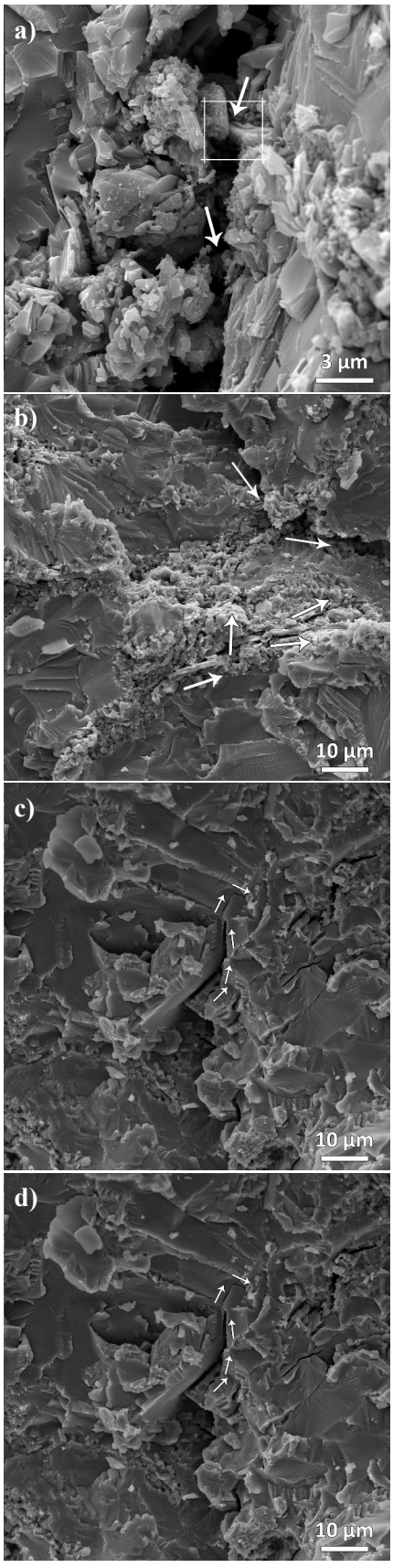

Fig. 9. SE-FESEM fractographs of a, b) sample 2 (reprinted with permission of Ref. [45]) and c, d) sample 4 tested by SENB method.

4. Conclusions

The effect of sintering conditions (SPS temperature and holding time) and Ti_3AlC_2 content on the physical and mechanical as-sintered TiAl-based composites was investigated. Densification of these materials was performed by spark plasma sintering of the elemental titanium and aluminum along with the synthesized Ti_3AlC_2 MAX phase. For this purpose, two samples with the composition of TiAl-15 wt% Ti_3AlC_2 composition and two other samples with the composition of TiAl-25 wt% Ti_3AlC_2 were prepared. One sample from each group was sintered once at 900 °C for 7 min under 40 MPa and again at 1000 °C for 15 min under 40 MPa. Increasing the sintering temperature and holding time had a positive effect on the relative density and mechanical properties, so that for the first group of samples: the relative density, Vickers hardness, fracture toughness, and bending strength reached 95.21%, 4.49 GPa, 11.98 MPa.$m^{1/2}$, and 336 MPa and for the second group of samples: the relative density, Vickers hardness, fracture toughness, and bending strength reached to 97.52%, 4.58 GPa, 11.81 MPa.$m^{1/2}$, and 340 MPa, respectively.

CRediT authorship contribution statement

Maryam Akhlaghi: Investigation, Data curation, Writing – original draft, Visualization.
Esmaeil Salahi: Project administration, Supervision, Methodology.
Seyed Ali Tayebifard: Conceptualization, Funding acquisition, Validation.
Gert Schmidt: Writing – review & editing.

Data availability

The data underlying this article will be shared on reasonable request to the corresponding author.

Declaration of competing interest

The authors declare no competing interests.

Funding and acknowledgment

The content of this article is based on the PhD thesis of the first author. The authors would like to express their gratitude to the Materials and Energy Research Center for its support of this research project under grant number 481394051. Additionally, the invaluable assistance of Dr. Behzad Nayebi in result analysis and Mrs. Masoumeh Enayati and Mrs. Nadi Shojaei in conducting the experiments is sincerely appreciated.

References

[1] H. Huang, H. Ding, X. Xu, R. Chen, J. Guo, H. Fu, Phase transformation and microstructure evolution of a beta-solidified gamma-TiAl alloy, J. Alloys Compd. 860 (2021) 158082. https://doi.org/10.1016/j.jallcom.2020.158082.

[2] Z. Trzaska, G. Bonnefont, G. Fantozzi, J.-P. Monchoux, Comparison of densification kinetics of a TiAl powder by spark plasma sintering and hot pressing, Acta Mater. 135 (2017) 1–13. https://doi.org/10.1016/j.actamat.2017.06.004.

[3] H.P. Lim, W.Y.H. Liew, G.J.H. Melvin, Z.-T. Jiang, A Short Review on the Phase Structures, Oxidation Kinetics, and Mechanical Properties of Complex Ti-Al Alloys, Materials (Basel). 14 (2021) 1677. https://doi.org/10.3390/ma14071677.

[4] Y. Jiang, Y. He, H. Gao, Recent progress in porous intermetallics: Synthesis mechanism, pore structure, and material properties, J. Mater. Sci. Technol. 74 (2021) 89–104. https://doi.org/10.1016/j.jmst.2020.10.007.

[5] A. Couret, G. Molénat, J. Galy, M. Thomas, Microstructures and mechanical properties of TiAl alloys consolidated by spark plasma sintering, Intermetallics. 16 (2008) 1134–1141. https://doi.org/10.1016/j.intermet.2008.06.015.

[6] X. Liu, Q. Lin, W. Zhang, C. Van Horne, L. Cha, Microstructure Design and Its Effect on Mechanical Properties in Gamma Titanium Aluminides, Metals (Basel). 11 (2021) 1644. https://doi.org/10.3390/met11101644.

[7] A. Mohammadnejad, A. Bahrami, L. Tafaghodi Khajavi, Microstructure and Mechanical Properties of Spark Plasma Sintered Nanocrystalline TiAl-xB Composites (0.0 <x<1.5 at.%) Containing Carbon Nanotubes, J. Mater. Eng. Perform. 30 (2021) 4380–4392. https://doi.org/10.1007/s11665-021-05773-6.

[8] H.P. Qu, P. Li, S.Q. Zhang, A. Li, H.M. Wang, The effects of heat treatment on the microstructure and mechanical property of laser melting deposition γ-TiAl intermetallic alloys, Mater. Des. 31 (2010) 2201–2210. https://doi.org/10.1016/j.matdes.2009.10.045.

[9] L. Xiang, F. Wang, J. Zhu, X. Wang, Mechanical properties and microstructure of Al2O3/TiAl in situ composites doped with Cr2O3, Mater. Sci. Eng. A. 528 (2011) 3337–3341. https://doi.org/10.1016/j.msea.2011.01.006.

[10] H. Clemens, A. Bartels, S. Bystrzanowski, H. Chladil, H. Leitner, G. Dehm, R. Gerling, F.P. Schimansky, Grain refinement in γ-TiAl-based alloys by solid state phase transformations, Intermetallics. 14 (2006) 1380–1385. https://doi.org/10.1016/j.intermet.2005.11.015.

[11] M. Akhlaghi, E. Salahi, S.A. Tayebifard, G. Schmidt, Role of Ti3AlC2 MAX phase on characteristics of in-situ synthesized TiAl intermetallics. Part II: Phase evolution, Synth. Sinter. 1 (2021) 211–216. https://doi.org/10.53063/synsint.2021.1453.

[12] N.F. Mogale, W.R. Matizamhuka, Spark Plasma Sintering of Titanium Aluminides: A Progress Review on Processing, Structure-Property Relations, Alloy Development and Challenges, Metals (Basel). 10 (2020) 1080. https://doi.org/10.3390/met10081080.

[13] H. Jabbar, A. Couret, L. Durand, J.-P. Monchoux, Identification of microstructural mechanisms during densification of a TiAl alloy by spark plasma sintering, J. Alloys Compd. 509 (2011) 9826–9835. https://doi.org/10.1016/j.jallcom.2011.08.008.

[14] M. Akhlaghi, E. Salahi, S.A. Tayebifard, G. Schmidt, Role of Ti3AlC2 MAX phase on characteristics of in-situ synthesized TiAl intermetallics. Part III: microstructure, Synth. Sinter. 2 (2022) 20–25. https://doi.org/10.53063/synsint.2022.2182.

[15] Y. Kozhakhmetov, M. Skakov, N. Mukhamedova, S. Kurbanbekov, S. Ramankulov, W. Wieleba, Changes in the microstructural state of Ti-Al-Nb-based alloys depending on the temperature cycle during spark plasma sintering, Mater. Test. 63 (2021) 119–123. https://doi.org/10.1515/mt-2020-0017.

[16] M. Cabibbo, A. Knaislová, P. Novák, F. Průša, C. Paoletti, Role of Si on lamellar formation and mechanical response of two SPS Ti–15Al–15Si and Ti–10Al–20Si intermetallic alloys, Intermetallics. 131 (2021) 107099. https://doi.org/10.1016/j.intermet.2021.107099.

[17] B.-A. Behrens, K. Brunotte, J. Peddinghaus, A. Heymann, Influence of Dwell Time and Pressure on SPS Process with Titanium Aluminides, Metals (Basel). 12 (2022) 83. https://doi.org/10.3390/met12010083.

[18] Z.M. Sun, Q. Wang, H. Hashimoto, S. Tada, T. Abe, Synthesis and consolidation of TiAl by MA–PDS process from sponge-Ti and chip-Al, Intermetallics. 11 (2003) 63–69. https://doi.org/10.1016/S0966-9795(02)00183-8.

[19] D. Wimler, J. Lindemann, T. Kremmer, H. Clemens, S. Mayer, Microstructure and mechanical properties of novel TiAl alloys

tailored via phase and precipitate morphology, Intermetallics. 138 (2021) 107316. https://doi.org/10.1016/j.intermet.2021.107316.
[20] H. Jabbar, J.-P. Monchoux, F. Houdellier, M. Dollé, F.-P. Schimansky, et al., Microstructure and mechanical properties of high niobium containing TiAl alloys elaborated by spark plasma sintering, Intermetallics. 18 (2010) 2312–2321. https://doi.org/10.1016/j.intermet.2010.07.024.
[21] Y. Su, Y. Lin, N. Zhang, D. Zhang, Microstructures and mechanical properties of TiAl alloy fabricated by spark plasma sintering, Int. J. Mod. Phys. B. 34 (2020) 2040036. https://doi.org/10.1142/S0217979220400366.
[22] X. Gu, F. Cao, N. Liu, G. Zhang, D. Yang, et al., Microstructural evolution and mechanical properties of a high yttrium containing TiAl based alloy densified by spark plasma sintering, J. Alloys Compd. 819 (2020) 153264. https://doi.org/10.1016/j.jallcom.2019.153264.
[23] Y.Y. Chen, H.B. Yu, D.L. Zhang, L.H. Chai, Effect of spark plasma sintering temperature on microstructure and mechanical properties of an ultrafine grained TiAl intermetallic alloy, Mater. Sci. Eng. A. 525 (2009) 166–173. https://doi.org/10.1016/j.msea.2009.06.056.
[24] T. Voisin, J.-P. Monchoux, M. Hantcherli, S. Mayer, H. Clemens, A. Couret, Microstructures and mechanical properties of a multi-phase β-solidifying TiAl alloy densified by spark plasma sintering, Acta Mater. 73 (2014) 107–115. https://doi.org/10.1016/j.actamat.2014.03.058.
[25] D. Zhu, L. Liu, D. Dong, X. Wang, Y. Liu, et al., Microstructure and compression behavior of in-situ synthesized Ti2AlC reinforced Ti-48Al-2Cr alloy with carbon nanotubes addition, J. Alloys Compd. 862 (2021) 158646. https://doi.org/10.1016/j.jallcom.2021.158646.
[26] S. Haji Amiri, M. Ghassemi Kakroudi, T. Rabizadeh, M. Shahedi Asl, Characterization of hot-pressed Ti3SiC2–SiC composites, Int. J. Refract. Met. Hard Mater. 90 (2020) 105232. https://doi.org/10.1016/j.ijrmhm.2020.105232.
[27] S. Haji Amiri, M. Ghassemi Kakroudi, N. Pourmohammadie Vafa, M. Shahedi Asl, Synthesis and Sintering of Ti3SiC2–SiC Composites through Reactive Hot-Pressing of TiC and Si Precursors, Silicon. 14 (2022) 4227–4235. https://doi.org/10.1007/s12633-021-01207-z.
[28] X.H. Wang, Y.C. Zhou, Layered Machinable and Electrically Conductive Ti2AlC and Ti3AlC2 Ceramics: a Review, J. Mater. Sci. Technol. 26 (2010) 385–416. https://doi.org/10.1016/S1005-0302(10)60064-3.
[29] B. Mei, Y. Miyamoto, Investigation of TiAl/Ti2AlC composites prepared by spark plasma sintering, Mater. Chem. Phys. 75 (2002) 291–295. https://doi.org/10.1016/S0254-0584(02)00078-0.
[30] F. Yang, F.T. Kong, Y.Y. Chen, S.L. Xiao, Effect of spark plasma sintering temperature on the microstructure and mechanical properties of a Ti2AlC/TiAl composite, J. Alloys Compd. 496 (2010) 462–466. https://doi.org/10.1016/j.jallcom.2010.02.077.
[31] C. Liu, Y. Wang, W. Han, T. Ma, D. Ma, Y. Zhang, Achieving Superior High-Temperature Strength and Oxidation Resistance of TiAl Nanocomposite through In Situ Semicoherent MAX Phase Precipitation, ACS Appl. Mater. Interfaces. 14 (2022) 8394–8403. https://doi.org/10.1021/acsami.1c21719.
[32] M. Akhlaghi, S.A. Tayebifard, E. Salahi, M. Shahedi Asl, G. Schmidt, Self-propagating high-temperature synthesis of Ti3AlC2 MAX phase from mechanically-activated Ti/Al/graphite powder mixture, Ceram. Int. 44 (2018) 9671–9678. https://doi.org/10.1016/j.ceramint.2018.02.195.
[33] M. Akhlaghi, E. Salahi, S.A. Tayebifard, G. Schmidt, Role of Ti3AlC2 MAX phase on characteristics of in-situ synthesized TiAl intermetallics. Part I: sintering and densification, Synth. Sinter. 1 (2021) 169–175. https://doi.org/10.53063/synsint.2021.1347.
[34] D. Demirskyi, H. Borodianska, D. Agrawal, A. Ragulya, Y. Sakka, O. Vasylkiv, Peculiarities of the neck growth process during initial stage of spark-plasma, microwave and conventional sintering of WC spheres, J. Alloys Compd. 523 (2012) 1–10. https://doi.org/10.1016/j.jallcom.2012.01.146.
[35] J. Zhu, W. Yang, H. Yang, F. Wang, Effect of Nb2O5 on the microstructure and mechanical properties of TiAl based composites produced by hot pressing, Mater. Sci. Eng. A. 528 (2011) 6642–6646. https://doi.org/10.1016/j.msea.2011.04.062.
[36] J. Cheng, S. Zhu, Y. Yu, J. Yang, W. Liu, Microstructure, mechanical and tribological properties of TiAl-based composites reinforced with high volume fraction of nearly network Ti 2 AlC particulates, J. Mater. Sci. Technol. 34 (2018) 670–678. https://doi.org/10.1016/j.jmst.2017.09.007.
[37] Y. Liu, W. Zhang, Y. Peng, G. Fan, B. Liu, Effects of TiAl Alloy as a Binder on Cubic Boron Nitride Composites, Materials (Basel). 14 (2021) 6335. https://doi.org/10.3390/ma14216335.
[38] L. Rangaraj, V. Kashimatt, Pooja, B. Suresha, Reaction, densification and mechanical properties of Ti 2 AlC x ceramics at low applied pressure and temperature, Int. J. Appl. Ceram. Technol. 19 (2022) 2807–2816. https://doi.org/10.1111/ijac.14064.
[39] J. Wang, N. Zhao, P. Nash, E. Liu, C. He, et al., In situ synthesis of Ti2AlC–Al2O3/TiAl composite by vacuum sintering mechanically alloyed TiAl powder coated with CNTs, J. Alloys Compd. 578 (2013) 481–487. https://doi.org/10.1016/j.jallcom.2013.06.109.
[40] M. Liu, J. Chen, H. Cui, X. Sun, S. Liu, M. Xie, Ag/Ti3AlC2 composites with high hardness, high strength and high conductivity, Mater. Lett. 213 (2018) 269–273. https://doi.org/10.1016/j.matlet.2017.11.038.
[41] Y. Liu, Z. Li, Y. Peng, Y. Huang, Z. Huang, D. Zhang, Effect of sintering temperature and TiB2 content on the grain size of B4C-TiB2 composites, Mater. Today Commun. 23 (2020) 100875. https://doi.org/10.1016/j.mtcomm.2019.100875.
[42] C.L. Yeh, C.Y. Ke, Y.C. Chen, In situ formation of TiB 2 /TiC and TiB 2 /TiN reinforced NiAl by self-propagating combustion synthesis, Vacuum. 151 (2018) 185–188. https://doi.org/10.1016/j.vacuum.2018.02.024.
[43] Z. Aygüzer Yaşar, A.M. Celik, R.A. Haber, Improving fracture toughness of B4C – SiC composites by TiB2 addition, Int. J. Refract. Met. Hard Mater. 108 (2022) 105930. https://doi.org/10.1016/j.ijrmhm.2022.105930.
[44] Y. Wang, M. Yao, Z. Hu, H. Li, J.-H. Ouyang, et al., Microstructure and mechanical properties of TiB2-40 wt% TiC composites: Effects of adding a low-temperature hold prior to sintering at high temperatures, Ceram. Int. 44 (2018) 23297–23300. https://doi.org/10.1016/j.ceramint.2018.09.048.
[45] M. Akhlaghi, E. Salahi, S.A. Tayebifard, G. Schmidt, Role of Ti3AlC2 MAX phase on characteristics of in-situ synthesized TiAl intermetallics. Part IV: mechanical properties, Synth. Sinter. 2 (2022) 99–104. https://doi.org/10.53063/synsint.2022.22103.